Neural Networks 141 (2021) 184–198

Contents lists available at ScienceDirect

Neural Networks

journal homepage: www.elsevier.com/locate/neunet

Emulation of wildland fire spread simulation using deep learning

Frédéric Allaire [a,b,*], Vivien Mallet [a,b], Jean-Baptiste Filippi [c]

[a] Institut national de recherche en informatique et en automatique (INRIA), 2 rue Simone Iff, Paris, France
[b] Sorbonne Université, Laboratoire Jacques-Louis Lions, France
[c] Centre national de la recherche scientifique (CNRS), Sciences pour l'Environnement – Unité Mixte de Recherche 6134, Università di Corsica, Campus Grossetti, Corte, France

ARTICLE INFO

Article history:
Received 16 November 2020
Received in revised form 28 February 2021
Accepted 5 April 2021
Available online 20 April 2021

Keywords:
Deep neural network
Hybrid architecture
Mixed inputs
Numerical simulation
Fire growth prediction
Corsica

ABSTRACT

Numerical simulation of wildland fire spread is useful to predict the locations that are likely to burn and to support decision in an operational context, notably for crisis situations and long-term planning. For short-term, the computational time of traditional simulators is too high to be tractable over large zones like a country or part of a country, especially for fire danger mapping.

This issue is tackled by emulating the area of the burned surface returned after simulation of a fire igniting anywhere in Corsica island and spreading freely during one hour, with a wide range of possible environmental input conditions. A deep neural network with a hybrid architecture is used to account for two types of inputs: the spatial fields describing the surrounding landscape and the remaining scalar inputs.

After training on a large simulation dataset, the network shows a satisfactory approximation error on a complementary test dataset with a MAPE of 32.8%. The convolutional part is pre-computed and the emulator is defined as the remaining part of the network, saving significant computational time. On a 32-core machine, the emulator has a speed-up factor of several thousands compared to the simulator and the overall relationship between its inputs and output is consistent with the expected physical behavior of fire spread. This reduction in computational time allows the computation of one-hour burned area map for the whole island of Corsica in less than a minute, opening new application in short-term fire danger mapping.

1. Introduction

A major purpose of mathematical modeling and numerical simulation of wildland fire spread across land is to make relevant predictions and support long-term to short-term planning of fire-fighting actions. Fundamentally, fire spread implies heat transfer at scales of the centimeter, which is too computationally intensive to solve in operational conditions. Alternatively, fire spread modeling can be approached by solving a front-tracking problem where we focus on the propagation of the interface between burned and not burned areas, aka the *fire front*, over a 2D domain that represents the landscape. The growth of the burned surfaces from their initial state is governed by equations involving a model of rate of spread (ROS), that is to say the speed at which the flames advance, which is expressed as a function of local environmental parameters. Among such solvers, marker methods consist in discretizing the fire front by means of markers, which evolve in space and time according to an underlying fire behavior model that determines the speed at which the markers advance as well as other characteristics such as reaction intensity. Notable examples of simulators using this method include FARSITE (Finney, 1998), Prometheus (Tymstra, Bryce, Wotton, Taylor, & Armitage, 2010), and Phoenix (Tolhurst, Shields, & Chong, 2008), that are commonly used in the US, Canada, and Australia, respectively. Alternatively, level-set methods (e.g. Mallet, Keyes, & Fendell, 2009; Rochoux, Ricci, Lucor, Cuenot, & Trouvé, 2014) can be used in simulations to track the fire front, and other approaches were proposed to model fire spread, such as cell-based simulations (e.g. Johnston, Kelso, & Milne, 2008) that adopt a raster representation of the burned surface (see Sullivan, 2009b, for a detailed review of simulation models). Most of these approaches allow to simulate a fire propagating during more than an hour in a computational time of about a minute or less.

Physical models of wildland fire spread (Sullivan, 2009a), more complex and typically including heat transfer conservation laws, equations describing combustion chemistry, etc. have also been developed. However, their use is generally limited to research purposes, because the computational time for simulations based on such models is prohibitory in an operational context, even more so for large wildfires that may burn during several hours or even days and scale up to thousands of hectares.

* Corresponding author at: Institut national de recherche en informatique et en automatique (INRIA), 2 rue Simone Iff, Paris, France.
E-mail address: frederic.allaire@inria.fr (F. Allaire).

https://doi.org/10.1016/j.neunet.2021.04.006
0893-6080/

Evaluation of simulators of wildland fire spread can be carried out based on the comparison of an observed burned surfaces with its simulated counterpart. Several evaluation metrics have been proposed in wildland fire research, for instance relying on how much the two surfaces intersect (e.g. Duff, Chong, & Tolhurst, 2016; Filippi, Mallet, & Nader, 2013), on the distance between the vertices of the two fire perimeters (Duff, Chong, Taylor, & Tolhurst, 2012; Fujioka, 2002), or on information regarding the growth of the simulated and observed burned surfaces over time (Filippi et al., 2013). These metrics can be computed for observed fires, in which case the simulations can make use of data known in hindsight, such as fire suppression actions or observed weather variables (e.g. Duff et al., 2018; Salis et al., 2016), or be simply based on data available at the time of fire start (e.g. Filippi, Mallet, & Nader, 2014). ROS models, which may be involved in fire spread simulators, can also be evaluated based on observations obtained from laboratory or outdoor experiments or even from observed wildfires (Cruz & Alexander, 2014).

Given the complexity of wildland fires, there are significant uncertainty sources in modeling that may lead to considerable difficulties in determining the most appropriate decisions in an operational context (Thompson, Calkin, Scott, & Hand, 2017). In particular, for prediction purposes, there is considerable input uncertainty, which can refer to a range of possible values for a given model parameter or data source, possibly due to the use of weather forecasts or difficulty to estimate a single "best" value. In control theory, parameter uncertainty can be expressed by means of uncertainty matrices in the model (Zhou, Tao, Paszke, Stojanovic, & Yang, 2020) to design robust control laws (Stojanovic, He, & Zhang, 2020; Zhou, Tao, Paszke, Stojanovic, & Yang, 2020). The main goal of firefighters, once a wildfire has started (i.e. in a "crisis" situation), is to control the fire by means of suppression actions. These actions are difficult to model, therefore, predictions of wildland fire spread using simulators usually represent free spread (i.e. firefighting actions are not accounted for, but non-burnable areas such as water bodies may halt the progression of the fire front). Uncertainty can still be accounted for in such predictions, usually by propagating the probability distributions of the uncertain inputs following a Monte Carlo (MC) approach, resulting in an ensemble of fire spread simulations (e.g. Allaire, Filippi, & Mallet, 2020; Finney, Grenfell, McHugh, Seli, Trethewey, Stratton, et al., 2011; Pinto et al., 2016).

There are several possible applications of simulators of wildland fire spread in an operational context. As previously mentioned, in a crisis situation, they can help in predicting where the fire will spread and optimizing the fire suppression actions and evacuation. Prior to crisis situations, fire spread simulations are a major component of risk assessment frameworks to determine what areas have the highest potential to host a large incident. Wildland fire risk quantification generally involves models describing ignition probability, the probability for a given location to be burned, and the consequences on the objects affected by fire such as properties, timber production, as well as the consequences on human lives, wildlife habitats, etc. Several studies focused on fire risk mapping at the regional or country scale (Finney, McHugh, Grenfell, Riley, & Short, 2011; Lautenberger, 2017; Parisien et al., 2005), where many fires are simulated to represent a fire season or year according to some probabilistic distribution of ignition and environmental conditions driving fire spread. This process may be repeated hundreds of thousands of times as part of a Monte Carlo method. The purpose of such maps is to help in land management through the reduction of areas at risk in the long-term, by setting up fire breaks and providing more firefighting resources such as reservoirs, etc.

Regarding short-term planning, information for the next day or hours about the areas where a fire is most likely to ignite and how far the resulting fire may spread can be very useful in order to know what locations should be monitored more closely and help in anticipating the distribution of firefighting resources (firefighters, trucks, …) across the territory. For this purpose, one may focus on the quantification of "fire danger", a term that generally relates to the potential for ignition and spread of a fire at a given location. Traditional fire danger indices, widely used for decision support in an operational context, consist in a unitless value calculated essentially based on weather variables. A notable example of such an index is the Canadian Fire Weather Index (FWI Van Wagner & Pickett, 1985), used for generating maps of predicted fire danger covering Europe and the Mediterranean area as part of the European Forest Fire Information System (EFFIS).[1] Making use of output burned surfaces of wildland fire spread simulations offers an interesting alternative for quantifying fire danger: for instance, the resulting fire size accounts not only for weather but also for terrain (i.e. elevation and vegetation, which are also influential factors in fire spread) and can be expressed in hectares, a more "concrete" quantity. Numerical simulations of wildland fire spread could be used to generate high-resolution maps of fire spread on the basis of weather forecasts; but this would require numerous computations for different ignition locations, and the constraint on computational time would be too demanding even for simulators used for other operational purposes. As a rough estimate for the region considered in the present study, running one fire spread simulation with a computational of one minute for each hectare of land would amount to a computational time of 872,000 min (about 600 days) on a single processor, and even more if an ensemble of simulations is considered for each hectare; which would be too long even after distributing the computations on multiple processors.

In the aforementioned applications, and more particularly in short-term fire danger mapping, a promising approach to reduce computational time is to rely on an *emulator* (aka metamodel or surrogate model) to provide an approximation of some quantity of interest derived from the simulator's output. The idea is to focus on this quantity and compute it much faster with the emulator at the cost of some approximation error that should be as low as possible. Emulation may be used in situations when a fire spread model has high computational time and/or a lot of simulations or calls of a given function are required. Still, emulators are rarely used in wildland fire research even though their potential for reducing computational time of simulations appears desirable in this field. Examples include data assimilation of a fire front via polynomial chaos (Rochoux et al., 2014), sensitivity analysis through the computation of Sobol' indices related to the area and shape of the simulated burned surface with emulation by either Gaussian processes (GP) or generalized polynomial chaos (Trucchia, Egorova, Pagnini, & Rochoux, 2019), uncertainty quantification and computation of Sobol' indices regarding the ROS model of Rothermel (Rothermel, 1972) using high dimensional model representation methods (Liu, Hussaini, & Ökten, 2016), interpolation in a cell-based wildland fire spread simulator to quickly compute the values of correction factors in the relationship between advection velocity and spread angle on the basis of pre-computed values obtained in a few given configurations using a Radial Basis Function (RBF) approach (Ghisu, Arca, Pellizzaro, & Duce, 2015). Another example outside the scope of fire spread is the emulation of some outputs of a fire emission model with GP (Katurji et al., 2015).

Machine learning (ML) is a very rapidly growing area of study whose methods have been used for prediction and decision-making purposes in a variety of scientific and technical fields (Jordan & Mitchell, 2015). As exemplified by recent reviews, there has

[1] https://effis.jrc.ec.europa.eu/, last checked 2021.02.01.

been an increasing interest in application of ML to engineering risk assessment (Hegde & Rokseth, 2020), emergency management (Chen, Liu, Bai, & Chen, 2017), and to a wide variety of topics in wildland fire science (Jain et al., 2020) as well.

Neural networks, in particular, appear promising to take into account the complexity of wildland fire spread. For instance, an application involving emulation is proposed in Zhou, Ding, Ji, Yu, and Wang (2020) where a radial basis function neural network (RBFNN) is trained to emulate the similarity index between an observed burned surface and its simulated counterpart as a function of several ROS adjustment factors; a MC procedure is then applied to the emulator, providing parameter estimation of the adjustment factors for data assimilation of the simulated fire front. Other methods consist in using a convolutional neural network (CNN) as a surrogate for a wildland fire spread simulator to obtain a map of predicted burned areas (Hodges & Lattimer, 2019; Radke, Hessler, & Ellsworth, 2019). Data required to solve wildfire simulations have similarities with these involved in image processing as we are handling gridded maps of elevation and fuel parameters. As deep learning proved to be very appropriate to solve such image processing problems (Krizhevsky, Sutskever, & Hinton, 2012), it motivates the use of deep neural networks (DNNs) instead of traditional emulation techniques to approach emulation in wildland fire spread simulations.

In the present study, a method is proposed for the estimation of wildland fire spread in a wide variety of environmental conditions with potential for application to fire danger mapping. The quantity of interest is the burned surface area in hectares provided by a wildland fire simulator and the core of the method consists in the emulation of this output quantity using a DNN with a hybrid architecture so that both 2D and scalar input data are processed by specific layers. The present study focuses on Corsica island but the method can be extended to other regions.

The numerical simulator of wildland fire spread that is used as basis of the present work is presented in Section 2 together with the characteristics of the simulations. The strategy used to obtain the emulator is described in Section 3 and the results are provided and discussed in Section 4. Conclusions of this work are summarized in Section 5 where some perspectives of application of the emulator and possible extensions to the method are also mentioned.

2. Simulation of wildland fire spread

In the present study, wildland fire spread simulations are carried out with the numerical solver ForeFire (Filippi, Morandini, Balbi, & Hill, 2010). ForeFire relies on a front-tracking method where the fire front is represented by Lagrangian markers that are linked to each other by a dynamic mesh. The interface is discretized using an ordered list of Lagrangian markers at given locations on the surface of the Earth. The interface is then tracked by advecting all these markers at the propagation velocity of the front and by ensuring that the list of markers still holds an accurate representation of the interface. In this ordered list of markers, previous and next are defined by convention in the indirect direction as in Fig. 1. The outward normal defines the direction of propagation from burning regions toward unburned regions. Although fronts are allowed to contain islands of unburned fuel, they must remain simple polygons (with no self-intersection).

A key aspect of the simulation is the computation of rate of spread (ROS), that is to say the speed at which the flames advance. Several ROS models were proposed in the scientific literature. The model used in present study is the model of Rothermel (Rothermel, 1972), which is commonly used by fire managers in the US. The ROS is expressed as a function of several environmental properties such as wind speed, terrain slope, fuel

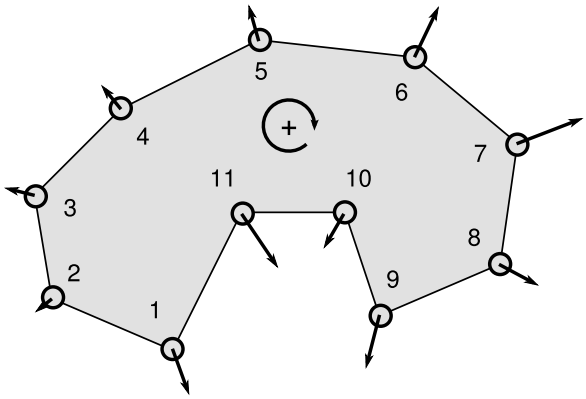

Fig. 1. Example of a small fire front discretization with ordered markers. The gray area in the center represents the burned surface and its interface with the unburned locations (white) represents the fire front whose vertices (markers) expand outward along the normal to the front.

moisture content (FMC), and other fuel parameters characterizing the vegetation. A simulation mostly consists in the definition of an initial state of the fire front and the ROS is computed for the markers of the fire front based on underlying 2D fields, from which environmental properties are determined. ForeFire relies on a discrete event approach where most computations deal with the determination of the time at which the markers will reach their next destination, this destination being defined by a fixed spatial increment in the outward normal. This discrete event approach includes other types of events such as changes in the values of the layers, notably wind speed and FMC, additions and removals of markers so that the fire front maintains a perimeter resolution in a given range during the simulation, and topology checks that may induce front merging to ensure that the front keeps a physical representation.

The area of study is Corsica island, which is located southeast of France in the Mediterranean sea. For fire simulation on this domain, 2D fields of elevation and land use in raster format at approximately 80-m resolution are used. These two fields are represented in Figs. 2(a) and 2(b). The land use field comes from Corine Land Cover data (Feranec, Soukup, Hazeu, & Jaffrain, 2016) coupled with data from the IGN (Institut Géographique National) product BD TOPO® for road and drainage networks. The elevation field is extracted from another IGN product: BD ALTI®, which originally has a 25-m resolution. A fuel parameterization is used to assign reference fuel parameters to each type of vegetation (referred to as "fuel type" in the following) in the land use data for ROS computations. Data used for simulation also include 2D fields of wind speed vectors at a resolution of 200 m that were pre-computed for average wind speed vectors with the mass conserving preconditioner from the atmospheric forecasting system Meso-NH (Lac et al., 2018) to account for orographic effects. By specifying an average input wind speed vector in the simulations, the underlying 2D wind field is simply obtained from the pre-computed fields corresponding to the closest mean speed vectors.

In the present study, a simulation is always that of a fire with free spread during one hour. Another fixed input in the simulations is the initial fire front, which is an octagon with a surface area of 0.45 ha, corresponding to an already-propagating fire, that must be located in areas classified as fuel (i.e. burnable vegetation) based on the land cover field.

Several inputs in the simulations may vary from a simulation to another. First are the coordinates of the center of the initial fire front, this point being referred to as the *ignition point*, that may

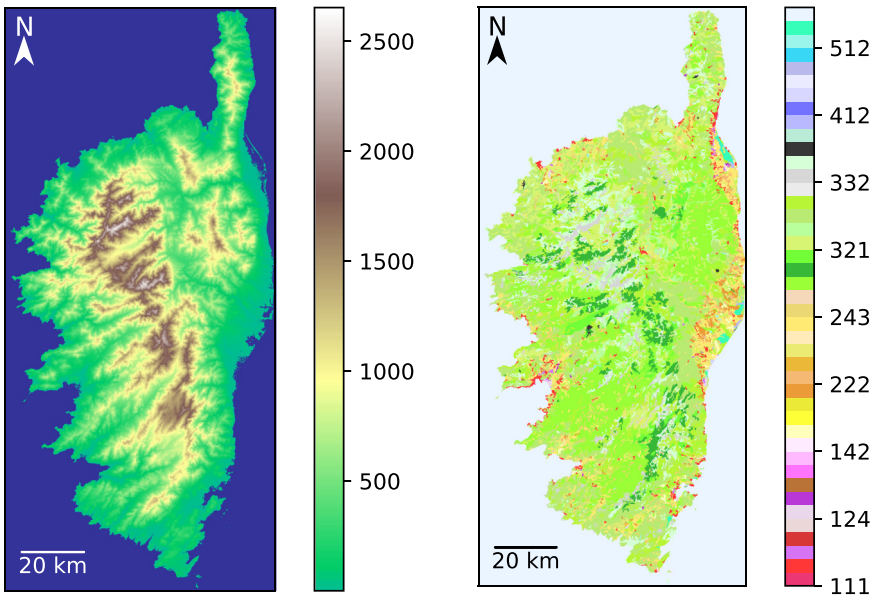

(a) Elevation field. (b) Land cover field.

Fig. 2. Data maps of Corsica used to describe the landscape in ForeFire simulations; their spatial resolution is approximately 80 m.
(a) Locations with an altitude of 0 m or less (mostly maritime waters) are represented in blue.
(b) The color scheme corresponds to the classification of the Corine Land Cover. (For interpretation of the references to color in this figure legend, the reader is referred to the web version of this article.)

be located in all fuel areas in Corsica. This "high-level" input is of major importance because it determines the location where the fire starts and the part of the spatial fields that will influence how the fire will spread. Next are the zonal and meridional coordinates of the "forcing" wind speed vector, in $m\,s^{-1}$, that both vary in $[-35, 35]$ on the condition that the wind speed norm be lower than $35\,m\,s^{-1}$. The FMC of dead fuel varies between 0.04 and 0.3. In contrast to these "raw" inputs, the remaining ones are perturbation coefficients that are applied to reference values of some fuel parameters. Perturbation in heat of combustion and particle density are additive and applied to a common reference value used for all fuel types, whereas perturbations in fuel height, fuel load or surface-volume ratio are multiplicative coefficients. For all the three latter parameters, each one of the 13 fuel types receives a specific perturbation coefficient. This amounts to 46 variable inputs in the simulations, whose information is summarized in Table 1, including the range of each variable.

The simulations are meant to be used for prevision of wildfire spread in Corsica before a fire starts, at any time, so the intervals of variation of the raw inputs were chosen to account for a wide variety of environmental conditions. Moreover, in this context, there is significant uncertainty in the simulations. The weather forecasts used to predict wind speed and FMC are possible sources of uncertainty, so are model simplifications and the choice of a given fuel parameterization. Therefore, the intervals of variation of both raw inputs and fuel parameters also account for their uncertainty range. Some intervals follow those of a previous study that focused on uncertainty quantification (see notably Table 1 in Allaire, Mallet, & Filippi, 2021).

Finally, the quantity of interest in the present study is the area in hectares of the burned surface obtained at the end of the simulation, namely after a free fire spread of one hour. An example of simulated surface is represented in Fig. 3.

It is possible with ForeFire to simulate any duration of fire and obtain the state of the fire front at any moment between fire start and fire end. Still, the simulated one-hour area alone could be a relevant information for the firefighters as it provides an estimation of the potential of fire growth if a fire that starts at a given location is not contained fast enough, one hour being a typical time for a fire to be detected and firefighters to arrive on-site.

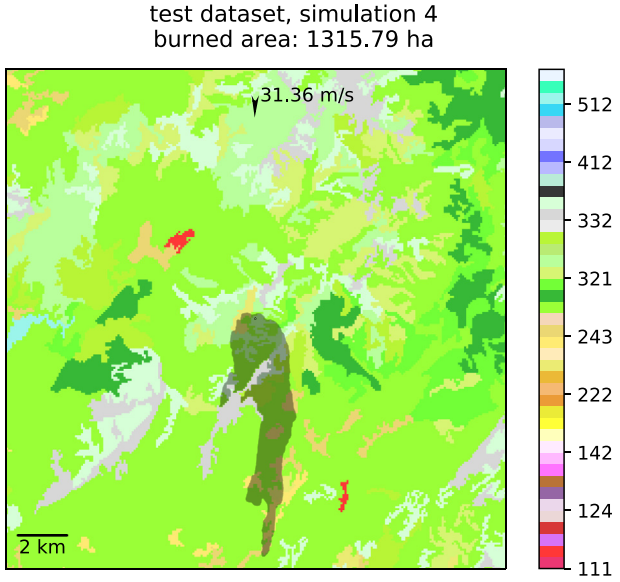

Fig. 3. Example of a simulated burned surface after one hour returned by ForeFire.
The initial fire front of 0.45 ha is represented in black at the center of the figure and the final burned surface is the surrounding shaded shape. The input wind speed vector is represented by the arrow at the top. The simulated fire spread to the south, was partly blocked by mountains (in gray), but still burned 1316 ha. Background colors correspond to the classification of the Corine Land Cover. (For interpretation of the references to color in this figure legend, the reader is referred to the web version of this article.)

Table 1
Variable scalar inputs in wildland fire spread simulations. In the case of perturbations, the symbol corresponds to the perturbed quantity, and the perturbation of this quantity can be either additive or multiplicative. The range indicates the boundaries of the domain of definition with two components for the wind and 13 components in the last three rows (one row per fuel type). The intervals of variation account for uncertainty and variability of weather and ignition locations, as well as for uncertainty.

Input	Symbol	Unit	Type	Range	Constraint
Ignition point coordinates	(x, y)	m	Raw	Map of Corsica	Initial front in burnable area
Wind speed	(W_x, W_y)	$\mathrm{m\,s^{-1}}$	Raw	$[-35, 35]^2$	Euclidean norm ≤ 35
Fuel moisture content (dead fuel)	m_c		Raw	[0.04, 0.3]	
Heat of combustion perturbation	ΔH	$\mathrm{MJ\,kg^{-1}}$	Additive	$[-5, 5]$	
Particle density perturbation	ρ_d	$\mathrm{kg\,m^{-3}}$	Additive	$[-300, 300]$	
Fuel height perturbations	h	m	Multiplicative	$[0.4, 1.6]^{13}$	
Fuel load perturbations	σ_f	$\mathrm{kg\,m^{-2}}$	Multiplicative	$[0.4, 1.6]^{13}$	
Surface-volume ratio perturbations	S_v	$\mathrm{m^{-1}}$	Multiplicative	$[0.4, 1.6]^{13}$	

3. Emulation with deep learning

In the context of fire growth prediction mentioned in Section 2, the absence of knowledge regarding the location of fire start and the uncertainty in the simulation are considerable difficulties that need to be addressed. An intuitive method consists in running a large number of simulations for ignition points all across the map, where some inputs are determined from weather forecasts. This procedure may or may not include perturbations in the inputs other than ignition point coordinates to account for uncertainty; but in any case, the time required to run all the desired simulations in operational conditions is too high with usual numerical simulators such as ForeFire. This motivates the use of an emulator to compute the area of the output simulated burned surface in a reasonable amount of time, although with some error of approximation. It is desirable to obtain an emulator that approximates this quantity with high accuracy and has a significantly lower computational time than that of the simulator, but it can be quite challenging for an emulator to combine both properties.

3.1. Design of experiments

A common strategy to design an emulator consists in considering the simulator as a "black-box" and build the emulator based on a synthetic dataset of input and corresponding output. The first step of this strategy is to define a design of experiments (DOE) to generate the datasets that will be used to build the emulator and evaluate its approximation error. Given input dimension and model complexity in the present study, we expect a large number of simulations ($\sim 10^5$ at the very least) will be required for an emulator to have good accuracy.

The DOE relies on a Latin Hypersquare Sample (LHS) in $[0, 1]^{46}$, which is a popular space-filling design. For all elements of the LHS, we apply an affine transformation from $[0, 1]^{46}$ to the hyperrectangle whose boundaries are defined by the ranges in Table 1. However, this procedure alone does not account for the restrictions to the definition domain implied by the constraints on ignition point coordinates and wind speed norm. To include these constraints, we generate a LHS with more members than n_{train}, the desired number of training sample members, and keep only "valid" members, namely those that satisfy the constraints after the affine transformation, so that the resulting sample size is slightly lower than the target. The next step in the constitution of the DOE is to generate a Sobol' sequence in $[0, 1]^{46}$, which is a low-discrepancy sequence. We complete the initial LHS (in $[0, 1]^{46}$) with members of the Sobol' sequence based on a discrepancy criterion, following the idea proposed in Iooss, Boussouf, Feuillard, and Marrel (2010) to obtain an optimal complementary design. A notable difference in the present study is that the first elements selected by the algorithm are used to complete the training sample only if they are valid (they are ignored otherwise). Then, when the target size n_{train} is reached, the next valid elements are used to form a test sample of size n_{test}. This procedure aims at selecting the points of the test sample so that they are located far from each other but also far from the points of the training sample, where the approximation error is expected to be higher.

Finally, based on the inputs of the training and test sample, the corresponding fire spread simulations are carried out as described in Section 2 and the resulting outputs complete the training and test datasets.

3.2. Neural network architecture

Several techniques can be considered for emulation. Simple statistical methods such as linear regression based on the inputs in Table 1 would most likely lead to poor approximation because of the non-linearity of the model. Other methods such as those mentioned in Section 1 (i.e. Gaussian processes, polynomial chaos, high dimensional model reduction, radial basis functions) are interesting alternatives, however their computational requirements (regarding time and/or memory space) can become prohibitory when there are both a high dimension ($d = 46$) and a large sample size ($\geq 10^5$).

In this problem, the input variables presented in Table 1 can be expressed as a vector of $\mathbb{R}^{46}$, including the coordinates (two scalars) of the ignition point. While these coordinates do locate the origin of the fire, they are not used directly to compute the ROS and simulate how the fire will spread from there. Actually, the restriction of the simulation domain to the surface that is burned after one hour identifies the part of the spatial fields of elevation and fuel parameters that were used in the ROS computations. Therefore, this information could be a better-suited emulator input than the coordinates of the ignition point. Although the simulated burned surface is not known beforehand, the fire will almost never spread further than 10 km in an hour, so *a priori* it will be contained in a 20 km $\times$ 20 km square centered around the ignition point. If one considers the fields of elevation and of fuel parameters h, σ_f, and S_v restricted to this square, given their 80-m spatial resolution, this amounts to four input fields of size 256 $\times$ 256 for emulation. This raises the need for a method that is adapted to handle such high-dimensional data as well as the remaining scalar inputs.

Neural network models appear suitable for emulation of fire spread simulations, not only because they usually perform well when trained on a large dataset, but also because they can handle several types of data. In particular, CNNs proved to be quite successful in the classification of 2D inputs such as images (e.g. Krizhevsky et al., 2012), but also for regression (e.g. Xie, Xing, Kong, Su, & Yang, 2015), which is our target. Here, the simulations are also significantly influenced by the other (scalar) inputs, notably wind speed and FMC, so a network with a hybrid architecture to process both types of inputs (2D and scalar) seems well suited to our problem. The term "hybrid" may have different

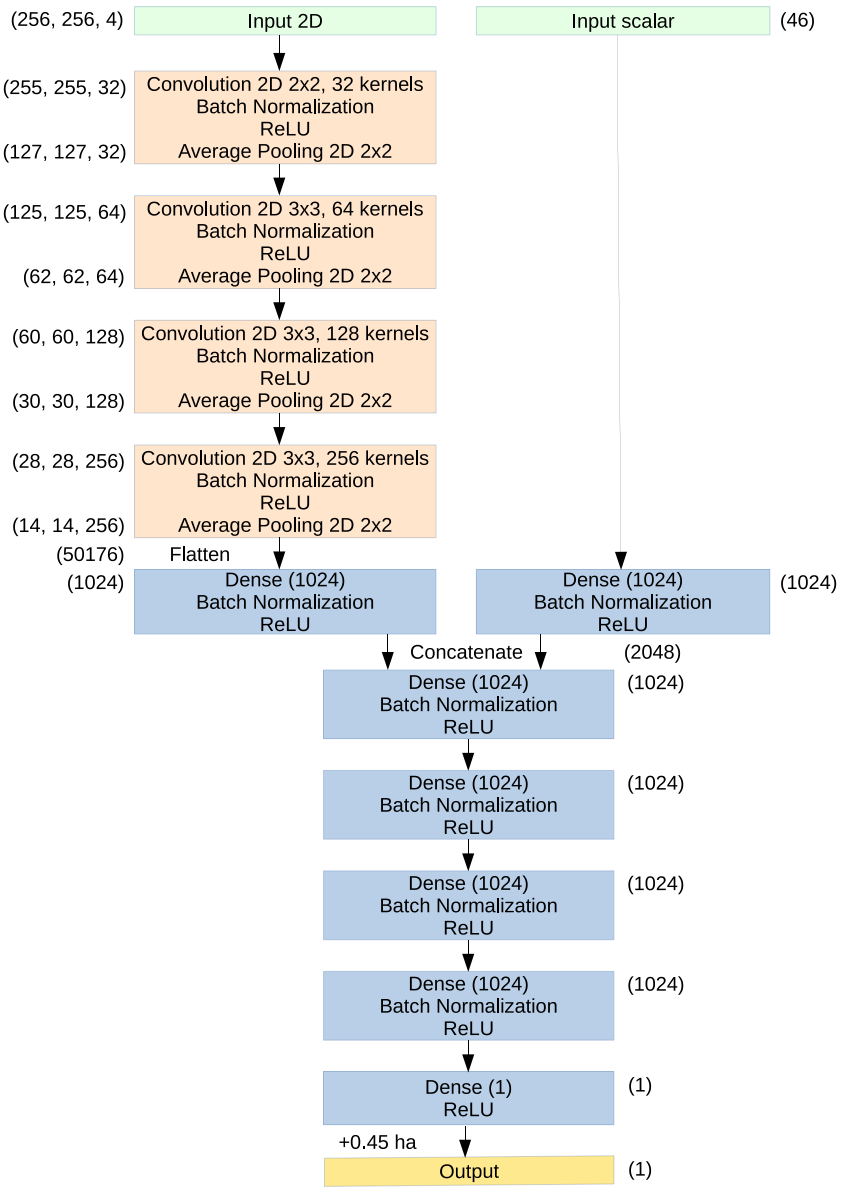

Fig. 4. Neural network architecture. The numbers in brackets outside the boxes indicate the shape of the data as they are processed by the network. The architecture is considered "hybrid" because the DNN processes both 2D input corresponding to terrain data and scalar inputs. Processing is first carried out separately until concatenation after which both parts are mixed.

meanings when it comes to neural networks. It can refer to the succession of multiple ensembles of layers, with each ensemble appearing like a given type of neural network, as in Quang and Xie (2016) where DNA sequences are first processed by a convolutional part then by a recurrent part. In the present study, this term is understood as the use of specific types of layers for each type of input, as proposed in Yuan, Jiang, Li, and Huang (2020) where image, sequential, and scalar/categorical inputs are first processed separately by the network.

We propose an emulator based on a DNN with a hybrid architecture. A convolutional part processes the four 2D fields of elevation and fuel parameters (prior to perturbation) h, σ_f, and S_v in a square surrounding the ignition point with a side of approximately 20 km, which corresponds to an input of shape (256, 256, 4). Another part of the network processes the vector of size 46 of scalar simulation inputs mentioned in Table 1. The "absolute" coordinates (x, y) of the ignition point are replaced by (δ_x, δ_y), which are the coordinates of this point relatively to the center of the surrounding 2D fields. Also, both 2D and scalar inputs are scaled to $[-1, 1]$ through an affine transformation before being processed by the DNN.

The detailed architecture of the DNN is represented in both Figs. 4 and 5. The first figure is more focused on the processing layers (i.e. convolutions, pooling, etc.), while the second figure represents the successive shapes of the data as they are processed by the network.

First, convolutions with a 2×2 window are applied to the 2D inputs, followed by a batch normalization layer, a Rectified Linear Unit (ReLU) activation and an average pooling layer with a 2×2 window. This succession of layers is repeated three more times, with a 3×3 window for the convolutions and more and more kernels. Convolutions are carried out without padding nor stride, and the first two average pooling layers result in the edge of the data being cropped, due to the odd input shape. Then, the output of these four blocks of layers is flattened and goes through a block consisting of a fully connected feed forward (aka dense) layer with 1024 output nodes, followed by batch normalization and ReLU activation. As for the scalar input, it goes through a similar

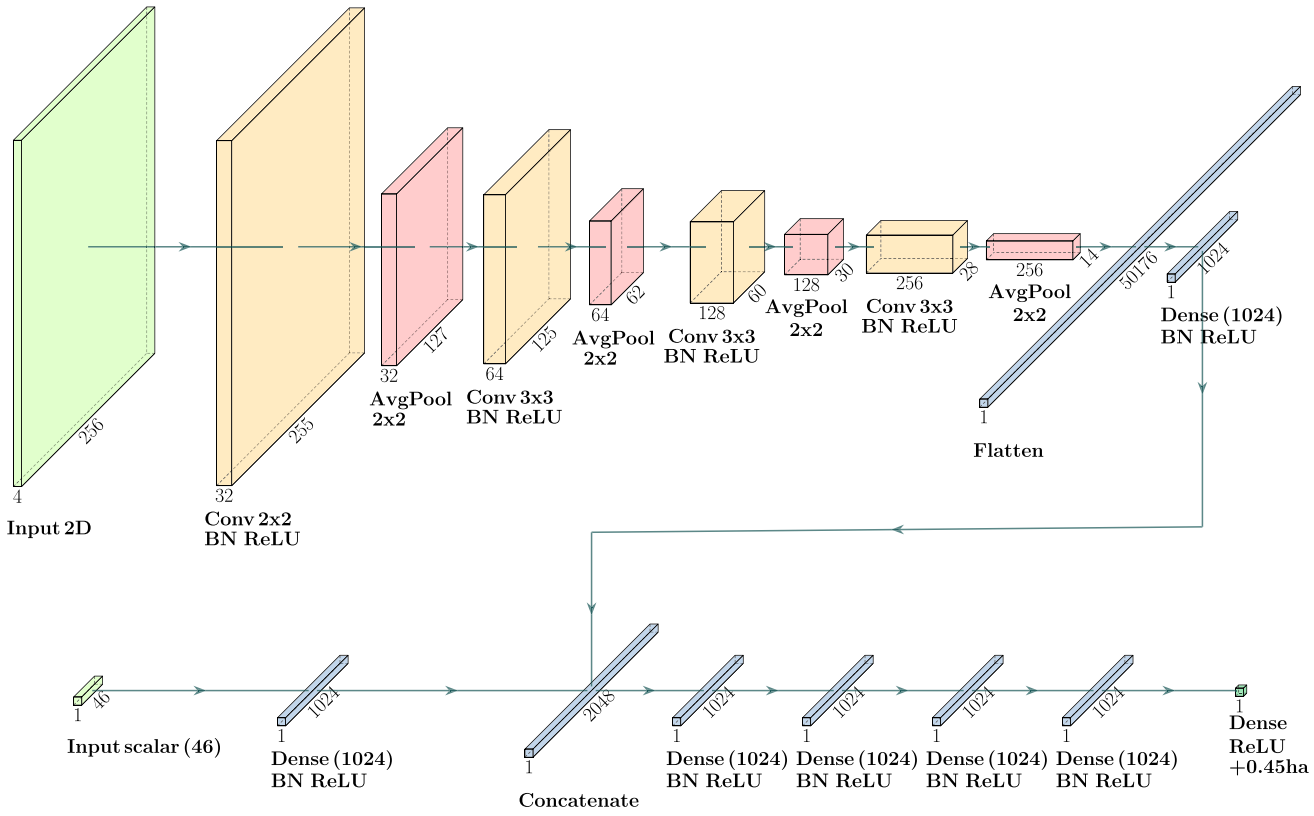

Fig. 5. Representation of data processing in the neural network. The blocks indicate the shape of the data. The 2D input is derived from the four fields of elevation, and fuel parameters h, σ_f, and S_v. The 46 scalar inputs are derived from the simulation parameter inputs of Table 1. Conv: Convolution 2D; BN: Batch Normalization; AvgPool: Average Pooling 2D.

block of layers. The output of these two blocks is concatenated and undergoes four similar blocks of layers. The intention behind the application of the dense blocks before concatenation is to concatenate vectors that have the same shape and potentially give similar importance to the 2D part and the scalar part in this mixed architecture. Finally, a dense layer followed by a ReLU activation and an increase of 0.45 ha (the minimum simulated burned surface area, corresponding to a fire that does not spread) are carried out, yielding the output of the network.

3.3. Accuracy metrics and training strategy

Among a dataset of size n, $\boldsymbol{u}^i$ denotes the ith set of simulation inputs, $y(\boldsymbol{u}^i)$ the resulting output, and $\tilde{y}(\boldsymbol{u}^i)$ the corresponding value returned by the emulator. Several metrics can be used to evaluate the accuracy of $\tilde{y}$, the emulator of function y. In this study, we use the mean absolute error (MAE), the mean absolute percentage error (MAPE), and the standardized mean square error (SMSE, cf. Rasmussen & Williams, 2006), which are respectively defined as follows:

$$\text{MAE} = \frac{1}{n}\sum_{i=1}^{n} |\tilde{y}(\boldsymbol{u}^i) - y(\boldsymbol{u}^i)|, \tag{3.1}$$

$$\text{MAPE} = \frac{1}{n}\sum_{i=1}^{n} \left|\frac{\tilde{y}(\boldsymbol{u}^i) - y(\boldsymbol{u}^i)}{y(\boldsymbol{u}^i)}\right|, \tag{3.2}$$

$$\text{SMSE} = \frac{\sum_{i=1}^{n}\left(\tilde{y}(\boldsymbol{u}^i) - y(\boldsymbol{u}^i)\right)^2}{\sum_{i=1}^{n}\left(y(\boldsymbol{u}^i) - \bar{y}\right)^2}, \tag{3.3}$$

where $\bar{y} = \frac{1}{n}\sum_{i=1}^{n} y(\boldsymbol{u}^i)$ is the sample mean of the emulated function. The SMSE can be seen as a mean squared error normalized by the sample variance of y, and would be equal to 1 if the emulator was a constant function equal to the sample mean $\bar{y}$. The lower these scores, the more accurate the emulator. The emulator can also be evaluated in terms of mean error, similarly to the MAE but without the absolute value, that will be referred to as "bias" in the following.

The accuracy metrics need to be computed for the test dataset as the error is expected to be much lower for the training dataset, which is used to determine the parameter values of the network. In order to quantify overfitting, the accuracy metrics may also be computed for the training dataset.

The procedure used to train the network's parameters relies on a MAE loss function with an Adadelta optimizer (Zeiler, 2012), without regularization based on the norm of the layer parameters.

To enrich the train dataset, a form of data augmentation is carried out: over one epoch, each member of the training dataset is used exactly once, but possibly after a geometric transformation (rotations or axial symmetries). The geometric transformation is applied to the 2D field inputs as well as (W_x, W_y), the wind speed vector, and (δ_x, δ_y), the relative coordinates of the ignition point. There is a 0.5 probability of having no transformation, whereas the other transformations (seven different non-identity applications) each have a 1/14 probability of being applied, all of them being represented in Fig. 6. We know that in such a configuration, the simulated burned surface would be the same, so this allows us to enrich the dataset (virtually, by a factor of eight) without running additional ForeFire simulations, and might limit overfitting (Shorten & Khoshgoftaar, 2019) since it allows for more possible configurations than described in Section 2. Note that data augmentation is only used during training. Also, with the synthetic datasets there is no need to split the training dataset to obtain a validation dataset, since the test dataset was designed specifically to evaluate accuracy, as explained in Section 3.1. The

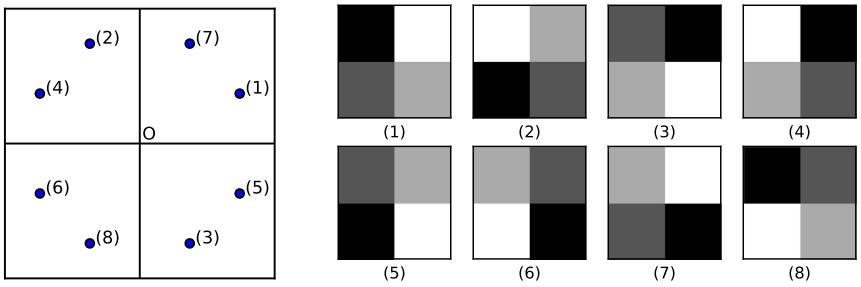

(a) Transformations applied to a point. (b) Transformations applied to a matrix.

Fig. 6. Geometric transformations used for data augmentation during training.
Considering (a) an initial point or vector in the plan with origin O or (b) a matrix in an initial state (1), 8 possible transformations are considered, resulting in state (n), with n $\in \{1, \ldots, 8\}$. Identity transformation, leading to (1), has a 0.5 probability of being applied during training. The probability is 1/14 for all other transformations. (2): 90° rotation, (3): −90° rotation, (4): y axis symmetry, (5): x axis symmetry, (6): 180° rotation, (7): y = x axis symmetry, (8): y = −x axis symmetry.
Applying one of these transformations to the input data would result in a similarly transformed simulated burned surface, so the output area in hectares is invariant to these transformations.

accuracy metrics of the network are simply computed for the test dataset at the end of each epoch during training.

3.4. Extraction of the actual emulator

The DNN presented in Section 3.2 relies on many convolutions that can be computed much faster with high-performance graphics cards. Even if one is not equipped with such resources, it is possible to compute the output of the DNN even faster once the network has been trained.

To achieve this goal, the final layer of the convolutional part of the network (of size 1024), before concatenation with the scalar part, is pre-computed. Indeed, due to the spatial resolution of the elevation and land cover fields of approximately 80 m, there is a finite amount of possibilities for the 2D input and the subsequent layers up to the end of the convolutional part, which will take the same values as long as the ignition point is located in a given cell of side ∼80 m. In the present case, there are $\sim 1.2 \times 10^6$ possibilities for Corsica.

The actual emulator consists in the remaining part of the DNN and its inputs are the pre-computed final layer of the convolutional part as well as the scalar vector of size 46. This part of the network only involves some dense blocks and a concatenation of the two parts of the network, that can be computed much faster—even on a machine without specific acceleration.

3.5. Implementation

Python scripts are used to process the data, generate the training and test datasets, build and evaluate the DNN. Keras library, which is a high-level neural networks API that is running on top of TensorFlow, is used for building the DNN.

Training and accuracy evaluation of the DNN up to the retrieval of the actual emulator are carried out on a GPU accelerated compute node. The computational time of the actual emulator is evaluated on a machine with 32 CPU.

The size of the datasets are $n_{\text{train}} = 5 \times 10^6$ and $n_{\text{test}} = 10^4$. Training is carried out with data augmentation as explained in 3.3 for 100 epochs with batches of size 400, and the hyperparameters of the Adadelta optimizer are a decay rate of 0.95, a conditioning constant ϵ of 10^{-7}, and a learning rate of 0.3, which is an extra factor in the right-hand term of Equation (14) in Zeiler (2012). The weights of the network are initialized using default TensorFlow arguments, therefore the weights of Dense and Conv2D layers are initialized following a Glorot uniform initializer (cf. Equation (16) in Glorot & Bengio, 2010).

The same procedure is also applied to smaller training dataset of size $n_{\text{train}} \in \{10^5, 10^6\}$, each with a specific dataset of size $n_{\text{test}} = 10^4$ generated as explained in Section 3.1, to investigate the influence of n_{train} on the approximation error.

Table 2
Statistics of the output simulated burned surface area among the training dataset of size 5×10^6.
Std: Standard deviation; Q1: first quartile; Q3: third quartile.
The output has high variance, arguably making "relative" error metrics such as the MAPE and SMSE (cf. Eqs. (3.2) and (3.3), respectively) better suited for expressing the performance of the emulator regarding approximation error.

Mean	Std	Minimum	Q1	Median	Q3	Maximum
455.7 ha	782.0 ha	0.45 ha	52.6 ha	181.0 ha	517.7 ha	24 804.4 ha

4. Results and discussion

The computational time of a simulation (with ForeFire) of wildland fire spread took an average of approximately 25 s. This time highly depends on the input of the simulation and can range from about 0.1 s to more than an hour. Overall, the larger the simulated burned surface, the more computations are carried out during the simulation. Running all the simulations in the training and test datasets would have taken about 4 years if it were not for distributed computing: with several multi-CPU machines, for a total of about 150 CPU cores, the computations were completed in about 10 days. Given the simulation settings presented in Section 2, the obtained burned surface areas range from 0.45 ha to 24 804.4 ha among the training dataset. Some statistics of this output in the training dataset are presented in Table 2. The high variance of the simulation output is consistent with that of computational time. The minimum output corresponds to the area of the initial burned surface and is obtained in a few simulations (approximately half a thousandth) where the FMC is very close to the moisture of extinction (0.3) in the ROS model, leading to a fire that almost does not spread. Similar statistics are obtained with the test dataset, except for the maximum output (14 403.7 ha). The test dataset, having a much lower size than that of the training dataset, is less representative of the tail of the output distribution, hence the lower maximum.

Most simulations result in a burned surface of less than 1000 ha, which is realistic for a fire that spreads freely during

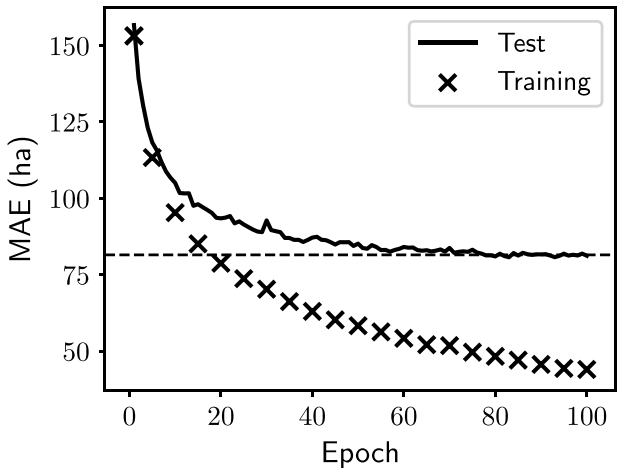

Fig. 7. MAE (loss function) over training. The solid curve represents the MAE for the test dataset, while the crosses represent the MAE computed for the training dataset at the end of the first epoch and after every five epochs starting from the fifth. The horizontal dotted line corresponds to MAE = 81.5 ha.
Both metrics decrease and this decrease is faster for the training dataset, yet the MAE for the test dataset does not increase and seems to keep around 81.5 ha after about 75 epochs. No significant decrease in the test error is expected after more epochs, so the network after 94 epochs, which has a SMSE on the test dataset of 6.0% (the best over all 100 epochs) is selected for emulation.

one hour. Still, a non-negligible amount of simulations result in burned surfaces that are most certainly bigger than what would be observed in reality. This amount would probably be higher were it not for non-burnable zones that significantly contribute to limit fire spread in some cases. This is mostly due to the fact that the simulations rely on simplifying assumptions where wind speed and FMC are constant in time and the DOE allows these inputs to vary in very large intervals. Therefore, it is not surprising to obtain a very large burned surface in a simulation where the wind speed is extremely high, the FMC extremely low, and no unburnable zone is reached during a whole hour of spread. Although somewhat unrealistic, the extremely high values of simulated burned surfaces were not removed from the dataset. This might make the emulation more difficult but the ability to discriminate between a wide range of situations, even extreme ones, is relevant in wildland fire spread.

Carrying out one epoch took a bit less than three hours, so training, which consisted in 100 epochs, lasted for about 10 days. The evolution of the MAE over training of the DNN for these 100 epochs is reported in Fig. 7. At a given epoch, the predicted values for both test and training datasets result from the model obtained at the epoch's end. Due to high computational time, the MAE was only computed for the training dataset (without applying data augmentation) at the first epoch and every five epoch starting from the fifth. On the one hand, the MAE for the test dataset decreases overall until it reaches 81.5 ha after about 78 epochs, after which it oscillates around that value. On the other hand, the MAE for the training dataset decreases overall, faster than the MAE of the test dataset. Therefore, while both scores are almost identical at the start, the gap between the two increases with the number of epochs.

The main objective is to have low generalization error, which is measured here using the error metrics for the test dataset. In high-dimensional cases, it is possible to observe a significant gap in error between the training and test datasets when training neural networks (see for instance Advani, Saxe, & Sompolinsky, 2020). It is the case in this study with the original model (ForeFire) relying on high-dimensional input data and being highly non-linear. Note that the neural network can be interpreted here as a substitute for an interpolator in high dimension, without the constraint to coincide with the training dataset at the training points.

Table 3
Model error on test dataset of size 10^4.
The approximation is poor using the three most simple models (constant and linear regression with or without threshold), whereas the DNN trained using a large training dataset shows good approximation.

Model \ Metric	MAE	MAPE	SMSE	Bias
Mean of training	461.9 ha	2266%	100.0%	2.2 ha
Linear regression without threshold	387.9 ha	1239%	73.9%	−4.8 ha
Linear regression with 0.45 ha threshold	361.1 ha	493.3%	72.3%	21.9 ha
DNN after 100 epochs	81.2 ha	33.5%	6.2%	−13.1 ha
Emulator (from DNN after 94 epochs)	81.2 ha	32.8%	6.0%	−6.5 ha

Table 4
Model error on training dataset of size 5×10^6.
For the three most simple models, the approximation metrics are almost the same to the ones computed on the test dataset (cf. Table 3), whereas the DNN has lower error for the training dataset than for the test dataset.

Model \ Metric	MAE	MAPE	SMSE	Bias
Mean of training	461.5 ha	2139%	100.0%	0 ha
Linear regression without threshold	389.9 ha	1185%	73.7%	0 ha
Linear regression with 0.45 ha threshold	365.6 ha	493.4%	72.3%	24.3 ha
DNN after 100 epochs	44.0 ha	23.8%	1.2%	−7.6 ha
Emulator (from DNN after 94 epochs)	45.1 ha	23.2%	1.2%	−0.9 ha

It is unlikely that carrying out more training epochs would result in a significant decrease of the error metrics for the test dataset. Consequently, the model with the best SMSE over the test set, which was obtained at the end of the 94-th epoch, was selected to define the emulator. The emulator with the best MAE was not selected because its MAE was only slightly lower (80.7 ha instead of 81.2 ha), whereas the other scores were all better for the model with the best SMSE. Even though our loss function (the MAE) may seem high, an absolute error of about 80 ha is at the same time very high for a small simulated burned surface of about 10 ha and very small for larger ones of about 1000 ha. Consequently, "relative" error metrics such as the MAPE and SMSE (cf. Eqs. (3.2) and (3.3), respectively) are arguably better suited for expressing the performance of the emulator regarding approximation error.

The error metrics of the emulator are reported in Tables 3 and 4, respectively relating to the test dataset and the training dataset. These metrics are also computed for three simple models for comparison: (1) a model that consists in always predicting the mean simulated burned surface of the training dataset (455.7 ha), (2) a linear regression model fitted using the training dataset based on the 46 inputs of Table 1, (3) same as the previous model, but applying a 0.45 ha minimum threshold (the minimum simulated area) to avoid non-physical output. The metrics for the DNN with the parameters obtained at the end of training are also reported. Although a MAE of 81.2 ha might seem high, it is much lower compared to that of the three simple models (461.9 ha with the mean, 361.1 ha for the linear regression with threshold). The SMSE of 6.0% means that 94.0% of the variance in the test dataset output is explained by the emulator, which is very good given the range of variation in simulation inputs. The relative error is also satisfactory with a MAPE of 32.8% on the test dataset, especially when compared to that of the simple models (2266.0% using the mean, 493.3% using linear regression with threshold). As for computational time on a 32-CPU machine, the outputs for the test dataset are obtained in about half a second with the emulator against 56 s with the whole DNN, which corresponds to a speed-up by a factor of about 100. Also, the corresponding ForeFire simulations would have been obtained in about two hours with parallel computations on the 32-CPU

Table 5
DNN error on complementary test dataset (always of size $n_{\text{test}} = 10^4$) with variable training dataset size n_{train}.
The larger the training dataset of the DNN, the better the approximation.

n_{train} \ Metric	MAE	MAPE	SMSE	Bias
10^5 (best SMSE after 34 epochs)	182.0 ha	89.1%	25.4%	−22.6 ha
10^6 (best SMSE after 26 epochs)	127.5 ha	49.9%	13.3%	−16.3 ha
5×10^6 (best SMSE after 94 epochs)	81.2 ha	32.8%	6.0%	−6.5 ha

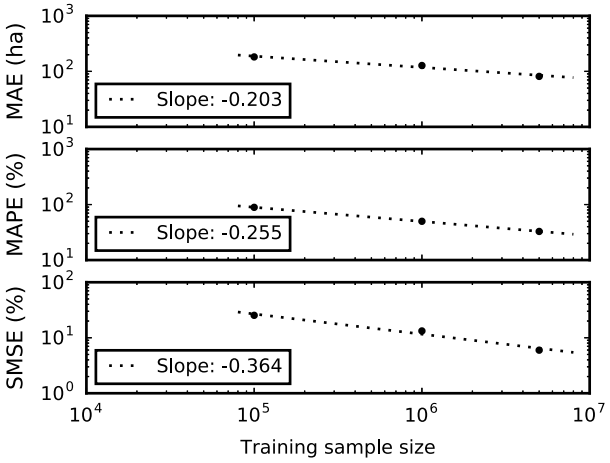

Fig. 8. Plot of the error metrics against n_{train} the size of the training dataset (cf. values reported in Table 5), in log scale.
Linear regression of the logarithms (dotted lines) results in a good fit with the data, suggesting a slowly decreasing trend of the form $(n_{\text{train}})^{-\alpha}$ with $\alpha \in [0.2, 0.37]$, depending on the metric.

machine, meaning that the emulator allows a speed-up by about 15,000 times. For a dataset where the simulated burned surface tends to be higher, the average computational time with ForeFire could be higher. This is not the case for the emulator, for which computational time does not depend on the output fire size, meaning that the resulting speed-up factor would be higher.

The influence of n_{train} on the resulting approximation error of the DNN based on the error metrics for the test dataset is presented in Table 5. The MAE in the test dataset did not seem to decrease after a few tens of epochs for smaller training datasets (this was also the case for $n_{\text{train}} = 5 \times 10^6$), and the model with best SMSE over 100 epochs, which had a MAE close to the best value obtained over the 100 epochs, was selected. Fig. 8 shows the MAE, MAPE, and SMSE from Table 5 plotted against n_{train}. Although there are only three points for each metric, linear regression of the logarithms suggests that the metrics decrease following a trend of the form $(n_{\text{train}})^{-\alpha}$ with $\alpha \in [0.2, 0.37]$, depending on the metric, which is quite slow. For instance, assuming this trend using the values of the slopes reported in Fig. 8 to specify α, reducing the MAE from 81.2 ha to 50 ha (resp. the MAPE from 32.8% to 20% and the SMSE from 6.0% to 2.0%) would require to increase n_{train} by approximately a factor 10 (resp. 7 and 20).

For more insight regarding the approximation of the selected model, the emulator output for each member of the test dataset is plotted against the actual values of simulated burned area in Fig. 9. The vast majority of the emulated values are close to their simulated counterparts and 9,332 out of 10,000 are at most either twice higher or half lower. In 157 cases, the emulator returns the minimum value of 0.45 ha, while the actual simulated value may go up to 10 ha. This corresponds to the apparent "black vertical bar" at the lower left of the graph in Fig. 9(a). There are 29 simulations for which the emulated burned area is at least five times lower (11 of them being equal to 0.45 ha) and 43 simulations for which the emulated value is at least five times higher. In the latter cases, most of the simulated burned surfaces are small ($\leq$10 ha in 32 simulations out of 43), which usually contributes to a higher relative error, but not all of them. In some of these cases of overprediction by the emulator, there is a relatively small area close to the ignition point in the main direction of fire spread that seems to considerably slow down the fire. The emulator probably has difficulty when it comes to accounting for some particular configurations of the underlying fuel and altitude fields, especially small non-burnable areas, given that the convolutional part of the DNN reduces the size of inputs by a factor of 256 when processing it for the emulator (from 262,144 to 1024). Overall, the individual errors lead to similar distributions of burned area. The emulator has a small bias of −6.5 ha and, as shown in Fig. 9(b), the histogram of emulated burned areas is slightly less dispersed (standard deviation of 752.9 ha against 782.5 ha).

The emulator is also evaluated with an ensemble of ForeFire simulations that correspond to a real Corsican fire that occurred near Calenzana during summer 2017 and burned about 120 ha. Most of the spread for this fire took place during the first hour after ignition. For this case, some reference inputs are defined from weather predictions and a presumed ignition point is identified, as explained in Allaire et al. (2020). Then, an ensemble of perturbed simulations is generated, for which the inputs presented in Table 1 follow a calibrated distribution that was obtained in a previous study (Allaire et al., 2021) with $\beta = 1/2$. It should be noted that the resulting ensemble of burned surface areas in the present study is not the same as in Allaire et al. (2021) because supplementary inputs were variable in the previous study (such as perturbations in the times of fire start and fire end, which could make the simulated fire duration different from one hour). The 10,000 simulated burned surface areas of the ensemble are compared to their emulated counterparts in Fig. 10. Similarly to the test dataset, most emulated values fall into the range of half to twice the simulated value, leading to a MAPE of 22.7%. A MAE of 18.7 ha is obtained and individual errors result in a distribution of the emulator output that is less dispersed than that of the simulated output, as shown in Fig. 10(b), with a bias of −9.6 ha and a standard deviation of 77.7 ha against 86.1 ha.

The overall agreement between simulation and emulation is good for this simulated fire case and the simulations were computed in 20 min, whereas the emulator predictions only took a bit more than a second. The speed-up factor is about 1000 this time, which is lower than the several thousands obtained for the test dataset. This is explained by the lower simulation time for this fire case (20 min instead of about two hours for the test dataset, while both datasets have the same size). This performance is quite promising for application to ensemble forecasting, but care should be taken as propagation of uncertainty leads to different output distributions according to the model (either ForeFire or its emulator) used.

Linked to the approximation error of the emulator is the influence of the inputs on the output. A desirable property of the emulator is the ability to behave in a similar way as ForeFire so that it keeps the main characteristics of the fire spread model, namely a burned area that, overall, increases with wind speed and decreases with FMC, while the surrounding 2D fields of altitude and fuel can either favor or block fire spread. Perturbations of fuel parameters are expected to have less influence, especially those of fuel parameters that are applied to a specific fuel type (h, σ_f, S_v). Also, the ROS is proportional to heat of combustion ΔH, which is a global parameter, so positive perturbations of this quantity will increase the burned area and negative ones will decrease it.

Given the complexity of the emulator, one may approach it as a black-box and estimate the overall influence of its inputs with

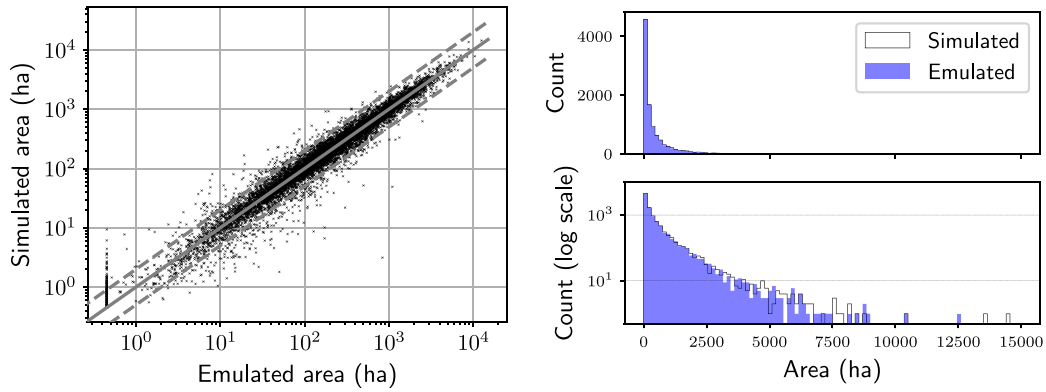

(a) Individual burned areas in log scale. (b) Histograms of burned areas.

Fig. 9. Comparison between the burned area simulated by ForeFire and the corresponding emulator output over the test dataset of size 10^4.
(a) The solid oblique gray line corresponds to a perfect match and the dotted lines correspond to an error by a factor of 0.5 and 2.
(b) Black contour: histogram of simulated areas; blue surface: histogram of emulated areas. Both top and bottom figures represent the same distributions, they share the same abscissa axis but the bottom figure has its ordinate in log scale.
Most of the emulated values are at most either twice higher or half lower, resulting in good error metrics (MAE=81.2 ha, MAPE = 32.8%), yet the individual error is quite high for a few members. The distributions of both samples are close. (For interpretation of the references to color in this figure legend, the reader is referred to the web version of this article.)

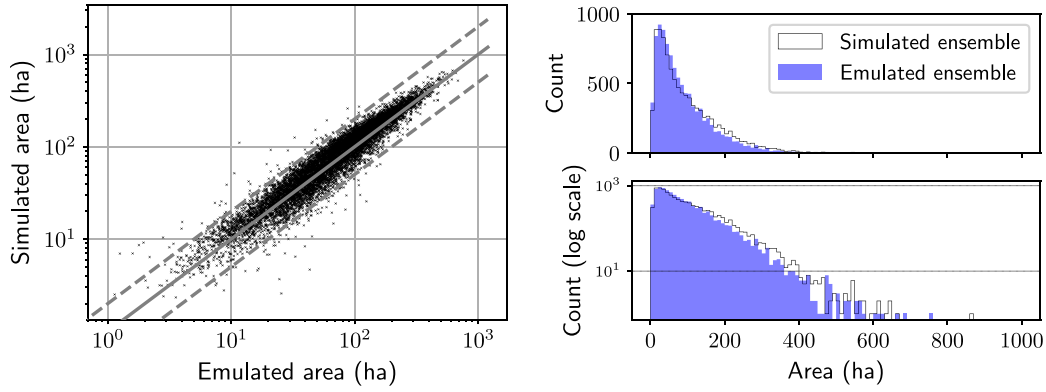

(a) Individual burned areas in log scale. (b) Histograms of burned areas.

Fig. 10. Comparison between the ensemble of burned areas simulated by ForeFire for the fire case of Calenzana and their emulated counterparts.
(a) The solid gray line corresponds to a perfect match and the dotted lines correspond to an error by a factor of 0.5 and 2.
(b) Black contour: histogram of simulated areas; blue surface: histogram of emulated areas. Both top and bottom figures represent the same distributions, they share the same abscissa axis but the bottom figure has its ordinate in log scale.
The inputs have smaller variations than for the test dataset, yet most emulated values fall into the range of half to twice the simulated value as it was the case for the test dataset (cf. Fig. 9), leading to good error metrics (MAE=18.7 ha, MAPE = 22.7%). (For interpretation of the references to color in this figure legend, the reader is referred to the web version of this article.)

Shapley additive explanations (SHAP, cf. Lundberg & Lee, 2017), a feature attribution method. The features we focus on are the inputs of the emulator, namely the 1024 "position" scalars linked to the 2D fields surrounding the ignition point stemming from the convolutions and the remaining 46 scalar inputs. Approximate SHAP values are computed for each member of the test dataset by means of expected gradients. This procedure leads to exact SHAP values when the model to explain is linear and the features are independent. While these assumptions are not verified with the emulator, the original algorithm for the computation of the exact SHAP values is too computationally expensive, whereas this method allows to compute approximate values in a reasonable amount of time. Although these results should be taken with care, they can still be used for a qualitative analysis and should provide some insight on the overall input influence over a whole dataset. For each member of the test dataset, the expected gradient is estimated based on a subset of size 50,000 sampled randomly from the training dataset. Given that the 1024 position scalars are difficult to interpret and expected to have little individual influence on the output due to their correlation, we consider the sum of their SHAP values, which is identified via a fictitious variable named "Position". The approximate SHAP values obtained for 12 of the 47 resulting variables are summarized in Fig. 11.

The values obtained for each of the 10,000 test members represented in Fig. 11(b) indicate a good overall agreement with the main characteristics of the fire behavior model. High FMC (m_c) tends to decrease the output while low FMC tends to increase it. High positive SHAP values for the coordinates of wind speed (W_x and W_y) are obtained for extreme values of these inputs, i.e. close to either $-35\,\mathrm{m\,s^{-1}}$ or $35\,\mathrm{m\,s^{-1}}$ (in blue and red, respectively) while the negative values are obtained for intermediate values (close to $0\,\mathrm{m\,s^{-1}}$). SHAP values associated to the perturbation of ΔH are also consistent with our expectations. Regarding the rankings of the inputs when looking at the absolute SHAP values averaged over the test dataset in Fig. 11(a), the three most influential inputs are the FMC and the two coordinates of the

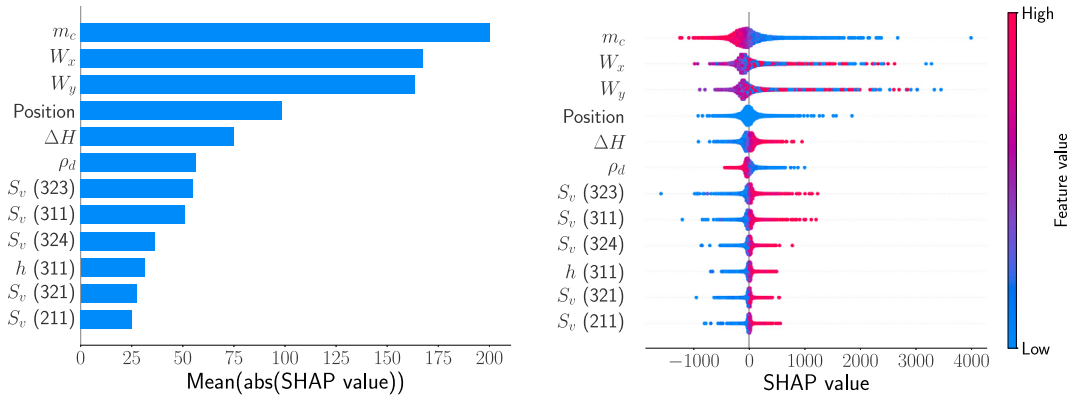

(a) Mean of the absolute value over the test dataset.

(b) Individual values for each member of the test dataset.

Fig. 11. Approximate SHAP values associated with the emulator computed for the test dataset, using the training dataset as basis. The SHAP values corresponding to the 1024 inputs resulting from the convolutional part of the DNN are summed up and this sum is identified as "Position" in the figure. Only the 12 most overall influential inputs, as ranked in (a), are represented.
(b) The color indicates the value of the input for each member, while the SHAP value is read in abscissa.
Qualitatively, the influence of the inputs expressed by the SHAP values corresponds to typical behavior of fire spread, both in terms of ranking and in terms of values for individual members (e.g. overall, low FMC m_c leads to a high SHAP value and high FMC leads to a low SHAP value). This suggests that the input–output relationship of the emulator is similar to that of the simulator. (For interpretation of the references to color in this figure legend, the reader is referred to the web version of this article.)

wind speed vector. Position is ranked fourth, perturbations on fuel parameters that affect all fuel types (ΔH and ρ_d) are ranked fifth and sixth, and the remaining ranks are attributed to the other perturbations of fuel parameters as well as δ_x and δ_y (ranked last). Interestingly, when the positional inputs are not summed, their individual influence is quite low: the 54th scalar of the vector of size 1024 is the highest ranked at rank 32 only. Although we only have an approximation of SHAP values, these results are qualitatively the ones we would expect from fire spread simulations and indicate that the emulator has an overall relationship between inputs and output that is fairly consistent with typical behavior of wildland fire spread.

The "physical" behavior of the emulator is also analyzed through the lens of fire danger mapping in Fig. 12 that represents the response surface of the emulator where the ignition point varies in Corsica, whereas the other inputs are fixed to $m_c = 0.13$, $(W_x, W_y) = (15, 15)\ \mathrm{m\,s^{-1}}$, and no perturbation on fuel parameters.

This mapping involves $\sim 1.2 \times 10^6$ emulator computations, which are carried out in about 40 s only. Values lower than 200 ha can be observed toward the south-west of non-burnable areas (mostly water bodies, rocky mountain tops over 1800 m with no vegetation, and urban areas), while most of the other ignition points are associated to values higher than 300 ha. This is consistent with the input wind speed vector pointing to the north-east. Also, there is a fairly high spatial variation of the emulated burned area that goes up to about 1500 ha. The smaller region shown in Fig. 12(b) presents some of the highest emulated values. Comparison with the underlying 2D fields of altitude and fuel used in the simulations does not reveal clear influence of either one of these fields on the emulated output (except for the ignition points to the south-west of non-burnable locations). An animated version of Fig. 12(a) with varying wind is available as Supplementary material. Considering that the approximation errors of the emulator are relatively low, it appears that, overall, the map generated using the emulator highlights locations where ignition would induce larger burned areas.

5. Conclusions

The basis for the present study was simulations of wildland fire spread with the numerical solver ForeFire using the underlying ROS model of Rothermel. These simulations represented free fire spread during one hour from a small initial burned surface located at all possible areas in Corsica island. The terrain was represented by 2D fields of fuel and altitude at approximately 80-m resolution in the simulations. Some environmental input parameters, namely FMC, wind speed, and perturbation of fuel parameters, were also allowed to vary in a wide range. ForeFire simulations can be computed in a reasonable amount of time, yet too high for applications that require a large number of simulations on a daily basis. This motivated the use of an emulator in order to faster compute an approximation of the output simulated burned area (in hectares).

The proposed approach consisted in training a DNN used for regression. The network has a hybrid architecture to deal with 2D fields of environmental parameters and with scalar inputs. On the one hand, the 2D fields are restricted to a square of 20 km side centered around the ignition point to filter out information that is, for the most part, not used during the simulation, and these fields go through convolutional blocks due to their similarity to images. On the other hand, the remaining scalar inputs go through a dense block and are concatenated with last layer of the convolutional part. Then, the rest of the network consists in more dense blocks. Training was carried out with a large dataset of size 5×10^6 obtained from a LHS sample, which could be augmented during training, and a complementary test sample of size 10^4 was obtained from a low-discrepancy sequence.

The DNN achieved good approximation of burned surface area simulated by ForeFire. The last layer of the convolutional part of the DNN for all fuel cells ($\sim 1.2 \times 10^6$) of the map of Corsica for which ignition is possible in the simulation is pre-computed. This allows to reduce computational time since the resulting positional information can be used together with the scalar inputs to run computations with only the remaining part of the DNN, which was chosen as emulator of burned surface area. The emulator

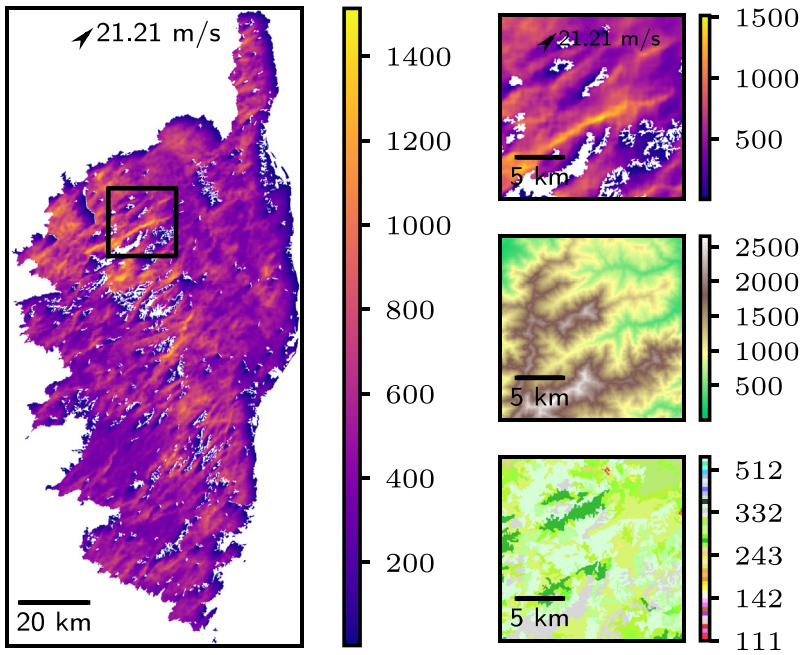

(a) Map of emulated burned area on the entire Corsica island.

(b) Zoom in the black square represented in (a).

Fig. 12. Map of the area (in hectares) of the burned surface predicted by the emulator with variable ignition point in Corsica. The other inputs are a wind speed vector of (15, 15) $\mathrm{m\,s^{-1}}$ represented with a black arrow, a FMC of 0.13, and no perturbation on fuel parameters. The spatial resolution is approximately 80 m; white pixels correspond to non-burnable locations in the simulations.
(b) From top to bottom: burned area (ha), altitude (m), land cover.
The "potential" area at a given ignition point is clearly lower when unburnable locations are close to the ignition point in the direction of the wind speed vector. This is consistent with "physical" behavior of wildland fire spread.

showed satisfactory performance. In the test dataset, it explains 94.0% of the variance of the output, it has a MAPE of 32.8%. Also, compared to the ForeFire simulations for fire danger mapping, the emulator computations are carried out thousands of times faster on a 32-CPU machine. Finally, the overall influence of the inputs on emulator output seems consistent with typical behavior of wildland fire spread.

Preliminary results suggest that the emulator is suited to ensemble predictions and fire danger mapping, notably due to the considerable speed-up factor. For instance, 1.2 million ForeFire simulations requiring 25 s on average would be computed in more than 10 days on a 32-CPU machine, while this took about 40 s with the emulator, that is to say more than 20,000 times faster.

Even though the DNN was trained for Corsica using ForeFire, the method presented in this work could be applied to other regions and/or similar fire spread simulators. In this method, the two most computationally expensive steps are (1) running the simulations required for the training dataset and (2) training the DNN. Thanks to high-performance computing resources (multi-CPU machines for the simulations and a GPU-accelerated core for training), both steps only took about 10 days in the present study. In other cases with bigger territories (e.g. at the scale of a country), one can expect that an even larger training dataset will be required to obtain comparable approximation error. Also, if the spatial resolution of the data maps is different, one may consider adapting the convolutional part. Regarding data size, the available RAM also poses a constraint on the batch size used during training. For these reasons, the authors strongly recommend using high-performance computing resource to apply the method and starting with a relatively small training dataset before moving on to a larger dataset. In spite of the high computational time for those two steps, once the DNN is trained and the emulator is obtained, the resulting speed-up factor should be worthwhile.

A major research perspective consists in evaluating the emulator for use in ensemble predictions and fire danger mapping, but now in a more extensive manner. In particular, actual weather forecasts that cover the whole island will be used to generate fire danger maps for every hour (at least) of a given day. This process can be carried by considering several real fire cases or an entire fire season. Depending on the ability of the emulator to quickly identify the locations with higher fire danger ahead of time, it could provide valuable help in an operational context.

Another perspective is to investigate how the DNN compares with other approximation techniques (regression or interpolation), but their application can be quite computationally expensive with large training datasets and may require to carry out data reduction on high-dimensional inputs. One may also focus on the neural network architecture to either increase its performance or extend its application to more scenarios of wildland fire spread simulations. A first extension could be to consider more simulation outputs, for instance the burned surface area every ten minutes after ignition. In this case, the DNN could yield a vector output that represents burned areas at different forecast times (instead of a single scalar) where each component could be expressed as the sum of the previous component plus a positive quantity. Similarly, inputs such as wind speed vector and FMC could vary during the simulation time. This would entail more possibilities in simulated scenarios, making the emulator more relevant for simulations of fires spreading during 1 hour or more, provided that it is trained with realistic weather time series, the definition of which is not obvious. As for network architecture,

upsampling layers could be considered hoping that they would re-constitute a good raster approximation of the burned surface. This burned surface could either be used directly as output (as in Hodges & Lattimer, 2019) or as the layer previous to the final output node estimating the number of hectares burned. Also, multi-dimensional recurrent neural networks (Graves, Fernández, & Schmidhuber, 2007) could be considered as substitute for the convolutional part of the DNN. Regardless of the complexity of the emulator, the main properties to pursue remain the same: low approximation error and reduction in computational time.

Declaration of competing interest

The authors declare that they have no known competing financial interests or personal relationships that could have appeared to influence the work reported in this paper.

Acknowledgments

Funding

This work was supported by the Agence Nationale de la Recherche, France [grant number ANR-16-CE04-0006 FIRECASTER].

Access to computing ressources

This work was carried out using HPC resources from GENCI-IDRIS (Grant 2020-AD011011630).

Appendix A. Supplementary data

Supplementary material related to this article can be found online at https://doi.org/10.1016/j.neunet.2021.04.006.

References

Advani, M. S., Saxe, A. M., & Sompolinsky, H. (2020). High-dimensional dynamics of generalization error in neural networks. *Neural Networks*, *132*, 428–446. http://dx.doi.org/10.1016/j.neunet.2020.08.022.

Allaire, F., Filippi, J.-B., & Mallet, V. (2020). Generation and evaluation of an ensemble of wildland fire simulations. *International Journal of Wildland Fire*, *29*(2), 160–173. http://dx.doi.org/10.1071/wf19073.

Allaire, F., Mallet, V., & Filippi, J.-B. (2021). Novel method for a posteriori uncertainty quantification in wildland fire spread simulation. *Applied Mathematical Modelling*, *90*, 527–546. http://dx.doi.org/10.1016/j.apm.2020.08.040.

Chen, N., Liu, W., Bai, R., & Chen, A. (2017). Application of computational intelligence technologies in emergency management: a literature review. *Artificial Intelligence Review*, *52*(3), 2131–2168. http://dx.doi.org/10.1007/s10462-017-9589-8.

Cruz, M. G., & Alexander, M. E. (2014). Uncertainty in model predictions of wildland fire rate of spread. In *Advances in forest fire research* (pp. 466–477). Imprensa da Universidade de Coimbra, http://dx.doi.org/10.14195/978-989-26-0884-6_54.

Duff, T. J., Cawson, J. G., Cirulis, B., Nyman, P., Sheridan, G. J., & Tolhurst, K. G. (2018). Conditional performance evaluation: Using wildfire observations for systematic fire simulator development. *Forests*, *9*(4), http://dx.doi.org/10.3390/f9040189, Retrieved from https://www.mdpi.com/1999-4907/9/4/189.

Duff, T. J., Chong, D. M., Taylor, P., & Tolhurst, K. G. (2012). Procrustes based metrics for spatial validation and calibration of two-dimensional perimeter spread models: A case study considering fire. *Agricultural and Forest Meteorology*, *160*, 110–117. http://dx.doi.org/10.1016/j.agrformet.2012.03.002.

Duff, T. J., Chong, D. M., & Tolhurst, K. G. (2016). Indices for the evaluation of wildfire spread simulations using contemporaneous predictions and observations of burnt area. *Environmental Modelling & Software*, *83*, 276–285. http://dx.doi.org/10.1016/j.envsoft.2016.05.005.

Feranec, J., Soukup, T., Hazeu, G., & Jaffrain, G. (2016). *European landscape dynamics: CORINE land cover data*. Boca Raton, USA: CRC Press.

Filippi, J.-B., Mallet, V., & Nader, B. (2013). Representation and evaluation of wildfire propagation simulations. *International Journal of Wildland Fire*, *23*, 46–57. http://dx.doi.org/10.1071/WF12202.

Filippi, J.-B., Mallet, V., & Nader, B. (2014). Evaluation of forest fire models on a large observation database. *Natural Hazards and Earth System Sciences Discussions*, *2*(11), 3077–3091. http://dx.doi.org/10.5194/nhessd-2-3219-2014, Retrieved from https://www.nat-hazards-earth-syst-sci.net/14/3077/2014/.

Filippi, J.-B., Morandini, F., Balbi, J. H., & Hill, D. R. (2010). Discrete event front-tracking simulation of a physical fire-spread model. *Simulation*, *86*(10), 629–646. http://dx.doi.org/10.1177/0037549709343117.

Finney, M. A. (1998). FARSITE: Fire Area Simulator-model development and evaluation. In *Res. pap. RMRS-RP-4, Revised 2004* (p. 47). Ogden, UT: U.S. Department of Agriculture, Forest Service, Rocky Mountain Research Station.

Finney, M. A., Grenfell, I. C., McHugh, C. W., Seli, R. C., Trethewey, D., Stratton, R. D., et al. (2011). A method for ensemble wildland fire simulation. *Environmental Modeling & Assessment*, *16*(2), 153–167. http://dx.doi.org/10.1007/s10666-010-9241-3.

Finney, M. A., McHugh, C. W., Grenfell, I. C., Riley, K. L., & Short, K. C. (2011). A simulation of probabilistic wildfire risk components for the continental United States. *Stochastic Environmental Research and Risk Assessment*, *25*(7), 973–1000. http://dx.doi.org/10.1007/s00477-011-0462-z.

Fujioka, F. M. (2002). A new method for the analysis of fire spread modeling errors. *International Journal of Wildland Fire*, *11*, 193–203. http://dx.doi.org/10.1071/WF02004.

Ghisu, T., Arca, B., Pellizzaro, G., & Duce, P. (2015). An optimal Cellular Automata algorithm for simulating wildfire spread. *Environmental Modelling & Software*, *71*, 1–14. http://dx.doi.org/10.1016/j.envsoft.2015.05.001.

Glorot, X., & Bengio, Y. (2010). Understanding the difficulty of training deep feedforward neural networks. In Y. W. Teh, & M. Titterington (Eds.), *Proceedings of machine learning research: vol. 9, Proceedings of the thirteenth international conference on artificial intelligence and statistics* (pp. 249–256). Chia Laguna Resort, Sardinia, Italy: JMLR Workshop and Conference Proceedings.

Graves, A., Fernández, S., & Schmidhuber, J. (2007). Multi-dimensional recurrent neural networks. arXiv preprint, arXiv:0705.2011.

Hegde, J., & Rokseth, B. (2020). Applications of machine learning methods for engineering risk assessment – A review. *Safety Science*, *122*, Article 104492. http://dx.doi.org/10.1016/j.ssci.2019.09.015.

Hodges, J. L., & Lattimer, B. Y. (2019). Wildland fire spread modeling using convolutional neural networks. *Fire Technology*, *55*(6), 2115–2142. http://dx.doi.org/10.1007/s10694-019-00846-4.

Iooss, B., Boussouf, L., Feuillard, V., & Marrel, A. (2010). Numerical studies of the metamodel fitting and validation processes. *International Journal on Advances in Systems and Measurements*, *3*, 11–21, Retrieved from https://hal.archives-ouvertes.fr/hal-00444666.

Jain, P., Coogan, S. C., Subramanian, S. G., Crowley, M., Taylor, S. W., & Flannigan, M. D. (2020). A review of machine learning applications in wildfire science and management. *Environmental Reviews*, http://dx.doi.org/10.1139/er-2020-0019.

Johnston, P., Kelso, J., & Milne, G. J. (2008). Efficient simulation of wildfire spread on an irregular grid. *International Journal of Wildland Fire*, *17*, 614–627. http://dx.doi.org/10.1071/WF06147.

Jordan, M. I., & Mitchell, T. M. (2015). Machine learning: Trends, perspectives, and prospects. *Science*, *349*(6245), 255–260. http://dx.doi.org/10.1126/science.aaa8415.

Katurji, M., Nikolic, J., Zhong, S., Pratt, S., Yu, L., & Heilman, W. E. (2015). Application of a statistical emulator to fire emission modeling. *Environmental Modelling & Software*, *73*, 254–259. http://dx.doi.org/10.1016/j.envsoft.2015.08.016.

Krizhevsky, A., Sutskever, I., & Hinton, G. E. (2012). ImageNet classification with deep convolutional neural networks. In F. Pereira, C. J. C. Burges, L. Bottou, & K. Q. Weinberger (Eds.), *Advances in neural information processing systems, vol. 25* (pp. 1097–1105). Curran Associates, Inc.

Lac, C., Chaboureau, J.-P., Masson, V., Pinty, J.-P., Tulet, P., Escobar, J., et al. (2018). Overview of the Meso-NH model version 5.4 and its applications. *Geoscientific Model Development*, *11*(5), 1929–1969. http://dx.doi.org/10.5194/gmd-11-1929-2018.

Lautenberger, C. (2017). Mapping areas at elevated risk of large-scale structure loss using Monte Carlo simulation and wildland fire modeling. *Fire Safety Journal*, *91*, 768–775. http://dx.doi.org/10.1016/j.firesaf.2017.04.014, Fire Safety Science: Proceedings of the 12th International Symposium.

Liu, Y., Hussaini, M. Y., & Ökten, G. (2016). Accurate construction of high dimensional model representation with applications to uncertainty quantification. *Reliability Engineering & System Safety*, *152*, 281–295. http://dx.doi.org/10.1016/j.ress.2016.03.021.

Lundberg, S. M., & Lee, S.-I. (2017). A unified approach to interpreting model predictions. In I. Guyon, U. V. Luxburg, S. Bengio, H. Wallach, R. Fergus, S. Vishwanathan, & R. Garnett (Eds.), *Advances in neural information processing systems, vol. 30* (pp. 4765–4774). Curran Associates, Inc.

Mallet, V., Keyes, D., & Fendell, F. (2009). Modeling wildland fire propagation with level set methods. *Computers & Mathematics with Applications*, *57*(7), 1089–1101. http://dx.doi.org/10.1016/j.camwa.2008.10.089.

M.S. Pinto, R., Benali, A., C.L. Sá, A., Fernandes, P. M., M.M. Soares, P., Cardoso, R. M., et al. (2016). Probabilistic fire spread forecast as a management tool in an operational setting. *SpringerPlus*, *5*, 1205. http://dx.doi.org/10.1186/s40064-016-2842-9.

Parisien, M., Kafka, V., Hirsch, K., Todd, J., Lavoie, S., & Maczek, P. (2005). *Mapping wildfire susceptibility with the BURN-P3 simulation model*: *Natural resources Canada, information report NOR-X-405*, Edmonton, Alberta: Canadian Forest Service, Northern Forestry Centre.

Quang, D., & Xie, X. (2016). DanQ: a hybrid convolutional and recurrent deep neural network for quantifying the function of DNA sequences. *Nucleic Acids Research*, *44*(11), e107. http://dx.doi.org/10.1093/nar/gkw226.

Radke, D., Hessler, A., & Ellsworth, D. (2019). FireCast: Leveraging deep learning to predict wildfire spread. In *Proceedings of the twenty-eighth international joint conference on artificial intelligence* (pp. 4575–4581). International Joint Conferences on Artificial Intelligence Organization, http://dx.doi.org/10.24963/ijcai.2019/636.

Rasmussen, C. E., & Williams, C. K. I. (2006). *Gaussian processes for machine learning*. The MIT Press.

Rochoux, M., Ricci, S., Lucor, D., Cuenot, B., & Trouvé, A. (2014). Towards predictive data-driven simulations of wildfire spread – Part I: Reduced-cost Ensemble Kalman Filter based on a Polynomial Chaos surrogate model for parameter estimation. *Natural Hazards and Earth System Sciences*, *14*(11), 2951–2973. http://dx.doi.org/10.5194/nhess-14-2951-2014.

Rothermel, R. C. (1972). A mathematical model for predicting fire spread in wildland fuels. In *Res. pap. INT-115* (p. 40). Ogden, UT: U.S. Department of Agriculture, Intermountain Forest and Range Experiment Station.

Salis, M., Arca, B., Alcasena, F., Arianoutsou, M., Bacciu, V., Duce, P., et al. (2016). Predicting wildfire spread and behavior in Mediterranean landscapes. *International Journal of Wildland Fire*, *25*, 1015–1032. http://dx.doi.org/10.1071/WF15081.

Shorten, C., & Khoshgoftaar, T. M. (2019). A survey on image data augmentation for deep learning. *Journal of Big Data*, *6*(1), http://dx.doi.org/10.1186/s40537-019-0197-0.

Stojanovic, V., He, S., & Zhang, B. (2020). State and parameter joint estimation of linear stochastic systems in presence of faults and non-Gaussian noises. *International Journal of Robust and Nonlinear Control*, *30*(16), 6683–6700. http://dx.doi.org/10.1002/rnc.5131.

Sullivan, A. L. (2009a). Wildland surface fire spread modelling, 1990 - 2007. 1: Physical and quasi-physical models. *International Journal of Wildland Fire*, *18*(4), 349–368. http://dx.doi.org/10.1071/wf06143.

Sullivan, A. L. (2009b). Wildland surface fire spread modelling, 1990 - 2007. 3: Simulation and mathematical analogue models. *International Journal of Wildland Fire*, *18*(4), 387–403. http://dx.doi.org/10.1071/wf06144.

Thompson, M., Calkin, D., Scott, J. H., & Hand, M. (2017). Uncertainty and probability in wildfire management decision support: An example from the United States. In K. Riley, P. Webley, & M. Thompson (Eds.), *Geophysical monograph*: *vol. 223*, *Natural hazard uncertainty assessment: Modelling and decision support* (1st ed.). (pp. 31–41). American Geophysical Union.

Tolhurst, K., Shields, B., & Chong, D. (2008). Phoenix: Development and application of a bushfire risk management tool. *Australian Journal of Emergency Management*, *23*(4), 47–54.

Trucchia, A., Egorova, V., Pagnini, G., & Rochoux, M. (2019). On the merits of sparse surrogates for global sensitivity analysis of multi-scale nonlinear problems: Application to turbulence and fire-spotting model in wildland fire simulators. *Communications in Nonlinear Science and Numerical Simulation*, *73*, 120–145. http://dx.doi.org/10.1016/j.cnsns.2019.02.002.

Tymstra, C., Bryce, R., Wotton, B., Taylor, S., & Armitage, O. (2010). *Development and structure of prometheus: The Canadian wildland fire growth simulation model*: *Natural resources Canada, information report NOR-X-417*, (p. 88). Edmonton, Alberta: Canadian Forest Service, Northern Forestry Centre.

Van Wagner, C. E., & Pickett, T. L. (1985). *Equations and FORTRAN program for the Canadian forest fire weather index system*: *Forestry technical report No. 33*, Ottawa: Environment Canada, Canadian Forestry Service, Petawawa National Forestry Institute.

Xie, Y., Xing, F., Kong, X., Su, H., & Yang, L. (2015). Beyond classification: Structured regression for robust cell detection using convolutional neural network. In N. Navab, J. Hornegger, W. M. Wells, & A. F. Frangi (Eds.), *Medical image computing and computer-assisted intervention* (pp. 358–365). Cham: Springer International Publishing.

Yuan, Z., Jiang, Y., Li, J., & Huang, H. (2020). Hybrid-DNNs: Hybrid deep neural networks for mixed inputs. arXiv preprint arXiv:2005.08419.

Zeiler, M. D. (2012). ADADELTA: An adaptive learning rate method. arXiv preprint arXiv:1212.5701.

Zhou, T., Ding, L., Ji, J., Yu, L., & Wang, Z. (2020). Combined estimation of fire perimeters and fuel adjustment factors in FARSITE for forecasting wildland fire propagation. *Fire Safety Journal*, *116*, Article 103167. http://dx.doi.org/10.1016/j.firesaf.2020.103167.

Zhou, L., Tao, H., Paszke, W., Stojanovic, V., & Yang, H. (2020). PD-type iterative learning control for uncertain spatially interconnected systems. *Mathematics*, *8*(9), 1528. http://dx.doi.org/10.3390/math8091528.